Cytochrome *c* in a Dry Trehalose Matrix: Structural and Dynamical Effects Probed by X-Ray Absorption Spectroscopy

Lisa Giachini,*† Francesco Francia,‡ Lorenzo Cordone,†§ Federico Boscherini,*† and Giovanni Venturoli†‡
*Dipartimento di Fisica, Università di Bologna, 40126 Bologna, Italy; †Consorzio Nazionale Interuniversitario per le Scienze Fisiche della Materia (CNISM), Italy; ‡Laboratorio di Biochimica e Biofisica, Dipartimento di Biologia, Università di Bologna, 40126 Bologna, Italy; and §Dipartimento di Scienze Fisiche ed Astronomiche, Università di Palermo, 90123 Palermo, Italy

ABSTRACT We report on the structure and dynamics of the Fe ligand cluster of reduced horse heart cytochrome *c* in solution, in a dried polyvinyl alcohol (PVA) film, and in two trehalose matrices characterized by different contents of residual water. The effect of the solvent/matrix environment was studied at room temperature using Fe K-edge x-ray absorption fine structure (XAFS) spectroscopy. XAFS data were analyzed by combining ab initio simulations and multi-parameter fitting in an attempt to disentangle structural from disorder parameters. Essentially the same structural and disorder parameters account adequately for the XAFS spectra measured in solution, both in the absence and in the presence of glycerol, and in the PVA film, showing that this polymer interacts weakly with the embedded protein. Instead, incorporation in trehalose leads to severe structural changes, more prominent in the more dried matrix, consisting of 1), an increase up to 0.2 Å of the distance between Fe and the imidazole N atom of the coordinating histidine residue and 2), an elongation up to 0.16 Å of the distance between Fe and the fourth-shell C atoms of the heme pyrrolic units. These structural distortions are accompanied by a substantial decrease of the relative mean-square displacements of the first ligands. In the extensively dried trehalose matrix, extremely low values of the Debye Waller factors are obtained for the pyrrolic and for the imidazole N atoms. This finding is interpreted as reflecting a drastic hindering in the relative motions of the Fe ligand cluster atoms and an impressive decrease in the static disorder of the local Fe structure. It appears, therefore, that the dried trehalose matrix dramatically perturbs the energy landscape of cyrochrome *c,* giving rise, at the level of local structure, to well-resolved structural distortions and restricting the ensemble of accessible conformational substates.

INTRODUCTION

Embedding biological structures into sugar amorphous matrices prevents damage from extreme environmental conditions such as exposure to high temperature and dehydration. Among sugars, trehalose appears to be the most effective in exerting a bioprotectant action (1–3). This disaccharide, composed of two $[1 \rightarrow 1]$-linked α,α units of glucopyranose, is synthesized by many organisms that can undergo anhydrobiosis, a condition enabling them to preserve their structural and functional integrity over several years of dehydration, surviving high temperatures ($>60°C$) and resuming their metabolic activity when rehydrated (4,5). When in anhydrobiosis, such organisms contain a large (up to 20% w/w) trehalose concentration.

Despite the great amount of attention devoted to this phenomenon, the molecular mechanisms by which carbohydrate matrices impart dehydration and temperature stability are still matters of intensive study; particularly elusive is the molecular basis of the peculiar efficacy of trehalose in bioprotection. According to the water-replacement hypothesis, stabilization occurs via the direct hydrogen bonding between the sugar and the biostructure (6). In a different model (water-entrapment hypothesis), residual water is supposed to concentrate close to the surface of the embedded macromolecule in the dried trehalose matrix (7). Viscosity effects inhibiting dynamic processes that lead to denaturation have also been invoked (8). According to this view, the peculiarity of trehalose has been put in relation to its rather high glass transition temperature with respect to other glass-forming sugars (9).

In the recent past, a large number of experimental and molecular dynamics (MD) studies have focused on protein-trehalose-water matrices. These studies, mainly performed on heme proteins, definitely established that in trehalose systems with low water content, internal protein dynamics are modulated by the content of residual water, being dramatically hindered in extremely dried matrices. Several spectroscopic studies, based on complementary techniques sensitive to atomic motion, support this view. Temperature-dependent optical absorption spectroscopy (10) showed that at room temperature incorporation of carboxymyoglobin (MbCO) into trehalose amorphous matrices reduces the amplitude of nonharmonic motions of Fe with respect to the heme plane. By exploiting Mössbauer spectroscopy (10) the same authors found that the onset of large-scale quasidiffusive motions of the Fe nuclei, which in the hydrated system appear at ~180 K (11), is shifted to ~230 K in dry trehalose matrices. Moreover, in the trehalose-coated protein, these motions are largely hindered even at room temperature. An analogous effect has been detected when measuring the

Submitted June 27, 2006, and accepted for publication November 1, 2006.

Address reprint requests to Giovanni Venturoli, Laboratorio di Biochimica e Biofisica, Dipartimento di Biologia, Università di Bologna, 40126 Bologna, Italy. E-mail: ventur@alma.unibo.it.

0006-3495/07/02/1350/11 $2.00

doi: 10.1529/biophysj.106.092338

protein hydrogen mean-square displacements in an extremely dry trehalose MbCO sample by elastic neutron scattering (12): again the large-scale motion that appeared at ~180 K in the hydrated protein (13) was hindered even at room temperature. Similar behavior has recently been observed in a neutron-scattering study performed on C-phycocyanin incorporated into a trehalose dry matrix (14).

These observations have been rationalized by MD simulations performed on a MbCO-trehalose-water system, which showed that 1), the amplitude of anharmonic motions stemming from the interconversion among the protein's conformational substates is greatly reduced in a trehalose matrix of low water content (15), and 2), in such systems, structures are formed in which the protein is confined within a network of hydrogen bonds connecting groups of the protein surface, water, and trehalose molecules. It has been proposed that these structures play a role in coupling the structure-dynamics of the protein to that of the matrix (16).

The occurrence of a tight dynamic and structural coupling within trehalose-water-MbCO structures has been further supported by the strict correlation observed between the thermal evolution (300–20 K) of the CO stretching and of the water association band in samples of MbCO embedded in trehalose matrices of different degrees of hydration (17).

In agreement with these observations, a recent study of spectral diffusion dynamics performed on trehalose-coated cytochrome (cyt) *c* suggests that in this heme protein also, diffusion-like motions are strongly reduced in trehalose matrices as compared to glycerol-water glasses and that the solvent changes some structural features of the protein (18).

These results have indicated that embedding a protein in a trehalose-water system can be a useful tool to investigate function-dynamics relations at room temperature as a function of the rigidity of the embedding matrix. This approach has been applied to both soluble and integral membrane proteins, making it possible to disentangle rigidity from temperature effects (for a review see Cordone et al. (19)). The results of these functional studies are consistent with the proposal that, in trehalose, protein dynamics are essentially conditioned by a hydrogen bond network that anchors the protein surface to the surrounding matrix. In particular, studies on the kinetics of electron transfer in bacterial photosynthetic reaction centers embedded in different amorphous matrices evidenced that the presence of trehalose in the matrix plays an essential role in hindering internal protein dynamics; in fact, it was shown that the reaction center dynamics coupled to electron transfer are only marginally affected in reaction center films dried in the absence of the sugar (20) or in polyvinyl alcohol (PVA) matrices (21), even at extremely low content of residual water. Studies performed in bacterial reaction centers have clearly shown that electron transfer processes involving different cofactors and occurring in different protein regions are differently inhibited by dehydration of the trehalose matrix (22), suggesting that specific, local protein dynamics are selectively modulated in the trehalose-water-protein system.

That incorporation of the protein into a trehalose matrix can cause subtle structural and dynamics changes localized to specific protein regions is also suggested by MD studies performed in parallel on an H_2O-solvated and on a trehalose-coated MbCO (15). By examining structure and dynamics effects specifically on the heme group, it was shown that although mean thermal fluctuations of the heme heavy atoms were decreased in the amorphous system at 300 K as compared to solution, the opposite occurred to the mean-square fluctuations of the heme H atoms, which exhibited a larger amplitude in trehalose. This observation, suggesting a different configuration of the heme in H_2O-solvated and trehalose-coated MbCO, has been put in relation with the finding that, in MD simulations of a trehalose-MbCO system, one trehalose molecule has been found in strong interaction with the heme propionate oxygen atoms (16).

As a whole, the results summarized above point out the necessity for a deeper knowledge of matrix-induced structural and dynamic effects at the local atomic scale. X-ray absorption fine structure (XAFS) spectroscopy appears to be particularly suited to provide such information, in view of its applicability to noncrystalline samples and of its high sensitivity in probing the local structure of a metal ion in a protein in the first few coordination shells (23,24). Because the XAFS function contains Debye-Waller factors, it can also yield information on the thermal fluctuations and static disorder that contribute to the relative mean-square displacements of the atoms (25). It is worthwhile to recall that XAFS measures only relative mean-square displacements between the absorbing and backscattering atoms, thereby providing information distinct from and complementary to that contained in the Debye-Waller factors determined by Mössbauer and by x-ray diffraction (26).

In this research, we have performed a comparative XAFS Fe K-edge study of cyt *c* in solution, in a weakly interacting matrix (PVA film), and in two trehalose matrices characterized by a different content of residual water. We have found that embedding the protein in the trehalose matrix leads to an increase in the bond length with an axial ligand and to a significant distortion of the porphyrin group, more pronounced in the more dehydrated system. In this strongly interacting matrix, we observed an impressive reduction of the mean-square relative displacements of the atomic correlations involving the central Fe and the first shell ligands.

MATERIALS AND METHODS

Sample preparation

Horse heart cyt *c* (Sigma-Aldrich, St. Louis, MO) was dissolved in 10 mM Tris buffer, pH 7.9. A molar excess of sodium ascorbate was added to fully reduce the heminic iron; the solution was eluted through a Sephadex G25 column (Amersham-Pharmacia PD10, Uppsala, Sweden), and the ascorbate-free ferrocyt *c* solution was used to prepare all the samples.

The concentration of ferrocyt *c* was evaluated spectrophotometrically on the basis of the reduced-oxidized absorbtion peak at 551 nm, using a differential extinction coefficient of 19.5 mM^{-1} cm^{-1}.

Starting from a 3.1 mM ferrocyt *c* stock solution, we prepared five samples characterized by different matrix environments for the protein: two liquid samples, a polyvinyl alcohol film, and two amorphous trehalose matrices differing in the extent of dehydration. The first liquid sample (sol. 1) was the stock solution itself; the other liquid sample (sol. 2) was obtained by addition of glycerol to produce a 40% v/v glycerol/water mixture. Solutions were inserted into 800-μl plastic cells with kapton windows. The ferrocyt *c*–containing PVA film (named PVA) was prepared by supplementing the stock solution with 2.5% w/v PVA (M_w ~130,000, Fluka, Buchs, Switzerland) and drying 1.4 ml of suspension (placed into a $3 \times 3 \times 0.3$ cm^3 Teflon holder) under N_2 flow. Ferrocyt trehalose samples were obtained by adding 147 mg of trehalose to 250 μl of stock solution to achieve a molar sugar/protein ratio of 500. A first sample (trehal. 1) was formed by layering the solution on a sintered boron nitride support and dehydrating it under dry N_2 flow for 3 h at room temperature. To obtain a more extensively dehydrated sample (trehal. 2), a sample prepared as described above was placed under high vacuum for 2 h and further dried under nitrogen flow for 8 h before x-ray measurements.

Data collection

Fe K-edge measurements were performed at the BM 8 GILDA beam-line of the European Synchrotron Radiation Facility (ESRF) in Grenoble, France. A Si(111) double crystal monochromator employing dynamic sagittal focusing (27) was used; the photon flux was of the order of 10^{11} photons per second, and the spot size was ~1×1 mm^2. Data were collected using a 13-element hyperpure Ge detector equipped with fast digital electronics with a peaking time equal to 1 μs (28). Samples were measured at room temperature in the region 6900–8200 eV. The edge region of each sample was recorded using an energy step of 0.1 eV to verify that in all samples the prepeak occurred at the same energy and had the same amplitude characteristic of the reduced form of cyt *c* (see Results and Discussion). Spectra are the average of multiple scans (from three to six), run consecutively on each sample.

XAFS model

It is well known that the local cluster around the iron center in cyt *c* (in both oxidized and reduced forms) is made up of a heme group, a histidine residue, and a methionine residue (29–37). In Table 1 we report the interatomic distances between iron and the first ligands for ferrocyt *c* from various species according to the Protein Data Bank (PDB). The significant variability in the interatomic distances reported might reflect real differences in the structure of cyt *c* from different organisms. However, it should be recalled that macromolecular crystallography and nuclear magnetic resonance (NMR) are unable to solve local structure details on the scale of 0.01-0.1 Å. Because we are interested in subtle structural changes induced by different matrices, an accurate starting model is highly desirable; we used the iron cluster atomic coordinates of horse heart ferrocyt *c* described by Cheng et al. (38) using multiple scattering analysis (MS) of XAFS data (obtained in a water-glycerol mixture at a 10 K temperature). The geometry of the cluster is shown in Fig. 1 *A*. The S_δ and $N_{\varepsilon 2}$ atoms of the methionine and histidine residues are on the axis (*z*) normal to the heme plane, and the histidine imidazole lies on the *x*-*z* plane. The values of distances and angles are reported in the figure caption. We note that in obtaining these values, constraints were applied to keep both the porphyrin and the imidazole group planar and to maintain a high symmetry in the heme structure (38,39).

Data analysis

The XAFS oscillations were extracted from the raw data using the AUTOBK program (40) as implemented in the ATHENA package (41), using a linear function for the preedge region and a cubic spline to mimic the atomic background. The data were analyzed using the ARTEMIS program (version 0.8.006) (41). Theoretical amplitude and phase shift functions were calculated using the ab initio code FEFF 8.2 (42). Scattering potentials were calculated by overlapping the free atom densities within the muffin tin approximation and then using the Hedin-Lundqvist form for the exchange potentials. The amplitude reduction factor (S_0^2) was calculated by FEFF 8.2 from atomic overlap integrals. This gave a value of 0.94, which has been kept fixed during the analysis.

In the reference structural model reported in Fig. 1, the most distant atom (C_β of methionine) is at 4.71 Å from the iron. It has been shown that in heme proteins atoms up to 5 Å from the iron center may give rise to significant MS contributions (43). Thus, all paths involving up to five scattering processes with an effective path length $\leq$5 Å were included for the fitting procedure (39,44).

The fits were performed directly in *k* space (with a *k* weight of 3) to avoid truncation and loss of information through Fourier filtering (26). The fitting range was 2.5–13 $Å^{-1}$ for all samples. As fitting parameters we used 1), a common shift in the energy origin, ΔE; 2), a number of distance variations to account for structural distortions; and 3), some Debye Waller (DW) factors, properly grouped in shells to account for the effect of thermal motion of the atoms (25) and/or structural disorder. As a goodness-of-fit index, we used the *R*-factor, defined as the sum of the squares of the differences between each experimental point and fit normalized to the sum of the squares of the experimental points.

To avoid overinterpretation of the data and to obtain a reliable estimate of structural and dynamical parameters, their number was reduced as described in the following: 1), we initially used rigid body refinement (45,46), introducing additional degrees of freedom only in a second step and only when necessary (see Results and Discussion); 2), in a first step rigid body refinement was performed with fixed values of DW factors; and 3), the DW factors of atoms at similar geometric positions were combined and successively varied only together (26,46).

Once the ligand distances obtained with fixed DW factors provided a satisfactory fit, the coordinates were fixed, and only the DW factors were varied together with a common shift in the energy origin (26). DW factors were grouped in the following manner. For the first neighbors, we introduced three DW parameters (one for the four pyrrolic nitrogens (N_p), one for the histidine nitrogen ($N_{\varepsilon 2}$), and the other one for the methionine sulfur (S_δ)). The appropriateness of considering two distinct Fe-N distances with individual DW factors (one for the four pyrrolic N_p and one for the histidine $N_{\varepsilon 2}$) was tested by fitting the EXAFS signal to simplified models characterized by 1), a single Fe-N bond length (and correspondent DW) common to the histidine and to the four pyrrolic nitrogens, and 2), two bond lengths (Fe-N_p and Fe-$N_{\varepsilon 2}$) with a jointly refined DW factor (see Results and

TABLE 1 First ligand distances for the iron site in ferrocytochrome *c* obtained from the PDB

PDB ID	Crystal/solution	Organism	Reference	Experimental method	Fe-N_p (Å)	Fe-$N_{\varepsilon 2}$ (Å)	Fe-S_δ (Å)
1KX2	Solution	Shevanella	Bartalesi et al. (37)	NMR	2.07	1.96	2.37
1GIW	Solution	Horse	Banci et al. (36)	NMR	2.08	1.94	2.36
2FRC	Solution	Horse	Qi et al. (35)	NMR	1.95	1.93	2.23
5CYT	Crystal	Tuna	Takano and Dickerson (30)	XRD	2.04	1.98	2.31
1CYC	Crystal	Bonito	Tanaka et al. (29)	XRD	1.81	2.60	2.49

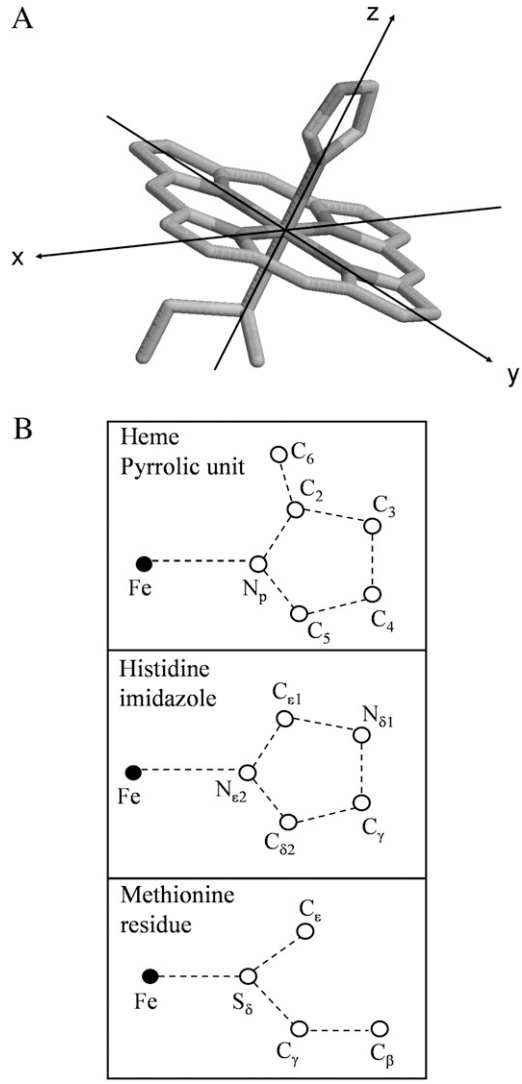

FIGURE 1 (*A*) Reference structural model of the Fe ligand cluster (38). (*B*) Sketch of the structural units of the reference model. The values of distances and angle are the following: Heme pyrrolic unit: Fe-N_p = 1.99 Å; N_p-$C_{2,5}$ = 1.38 Å; $C_{2,5}$-$C_{3,4}$ = 1.44 Å; C_3-C_4 = 1.34 Å; C_2-C_6 = 1.38 Å; Fe$N_pC_{2,5}$ = 109°; Fe$N_pC_{3,4}$ = 163°; $N_pC_2C_6$ = 125°; Histidine imidazole: Fe-$N_{\varepsilon 2}$ = 2.00 Å; $N_{\varepsilon 2}$-$C_{\varepsilon 1}$= 1.32 Å; $N_{\varepsilon 2}$-$C_{\delta 2}$= 1.37 Å; $C_{\varepsilon 1}$-$N_{\delta 1}$ = 1.34 Å; $C_{\delta 2}$-C_γ = 1.35 Å; C_γ-$N_{\delta 1}$ = 1.35 Å; Fe$N_{\varepsilon 2}C_{\varepsilon 1}$ = 128°; Fe$N_{\varepsilon 2}C_{\delta 2}$= 127°; Fe$N_{\varepsilon 2}N_{\delta 1}$ = 163°; Fe$N_{\varepsilon 2}C_\gamma$= 162°; Methionine residue: Fe-S_δ = 2.29 Å; S_δ-C_γ = 1.81 Å; S_δ-C_ε = 1.82 Å; C_γ-C_β = 1.5 Å; Fe$S_\delta C_{\varepsilon,\gamma}$ = 109°; $S_\delta C_\gamma C_\beta$ = 110°.

Discussion). For the more distant atoms, only the DW factors of the porphyrin group were allowed to vary in the fit, combined in three parameters (DW (C2) = DW (C5); DW (C6); DW (C4) = DW (C3)). All other DW factors were kept fixed at a value of 0.01 $Å^2$ (45).

In rigid body or constrained refinement, the number of parameters is reduced by treating a selected set of scattering atoms as a rigid unit. Following this approach, we considered as rigid structural units the imidazole ring, the methionine residue, and the heme pyrrolic unit (Fig. 1 *B*). As far as the porphyrin structure is concerned, a refinement of the first ligand distances together with the rigidity of the planar pyrrolic unit and the maintenance of the system symmetry imply that we are considering as the only structural degree of freedom the Fe out-of-plane axial displacement. In the case of histidine and methionine residues, along with the first ligand distances, angular parameters defining the bending on the *x-z* plane and twisting of the units around the $N_{\varepsilon 2}$ or S_δ atom (see Fig. 1 *A*) should also, in principle, be considered. However, for clusters containing a heme group, the XAFS signal is only weakly sensitive to the scattering paths that include atoms not belonging to the porphyrin ring. This makes the determination of the parameters of the axial ligands rather difficult (see Results and Discussion and Levina et al. (44)). In a first analysis, we refined, as structural parameters, only the first ligand distance of the imidazole ring and of the methionine residue, along with that of the four pyrrolic rings. Subsequently, the bending angles of the imidazole ring and of the methionine residue were also added to the free parameters. Including these additional parameters did not lead to a decrease of the R-factor (see Results and Discussion).

The structural degrees of freedom described above were sufficient to correctly reproduce the XAFS signals of the iron cluster in all samples except for the dried trehalose matrices. To account for the spectra measured in these samples, the constraint of rigid pyrrolic rings had to be released, and a minimum of three additional degrees of freedom in the heme structure were introduced (see Results and Discussion).

RESULTS AND DISCUSSION

In Fig. 2 we show the near edge region of the spectrum (XANES) of the sample in solution with glycerol (sol. 2); the spectra measured in the other samples (shown in Supplementary Material) are similar in this region. XANES features have been shown to give information on the oxidation state of cyt *c*. In fact, a shift to lower energy (~1 eV) of the edge transition has been observed in going from the ferricyt to the ferrocyt *c* form (38). Moreover, the preedge region exhibits a prepeak (see *inset* of Fig. 2) caused by the dipole-forbidden 1s → 3d transition, which occurs at slightly lower energy (7112 eV) in ferrous form (38). Also, the amplitude of the prepeak has been shown to be somewhat higher in the reduced state (38). The spectra of all our samples (see Fig. 2 and Supplementary Material, section 1.1) exhibit the typical XANES features reported for the reduced form of cyt *c*, with the pronounced prepeak centered at 7112 eV.

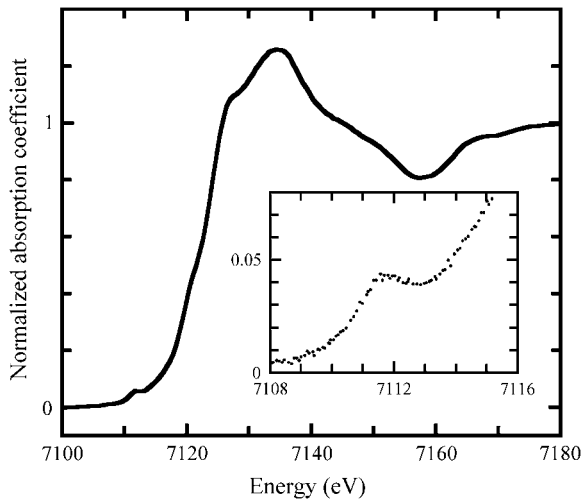

FIGURE 2 Edge and enlarged preedge (*inset*) spectra for ferrocytochrome *c* in solution with glycerol.

Multiple scans were run on each of the samples. To test the possible effects of radiation damage during the measurements, spectra recorded in consecutive runs were compared for each sample: no differences were found in any of the runs, particularly in the XANES region. To establish that no radiation damage had occurred during the first scan, optical spectra were measured after the XAFS measurements and compared with those of the nonirradiated ferrocyt *c* solution used to prepare all the samples. Nonliquid samples (PVA, trehal.1, and trehal.2) were redissolved with the proper amount of water after running the XAFS measurements. For all samples, optical spectra taken after irradiation are indistinguishable from those of the solution before measurement (see, e.g., the spectra recorded for sol. 1 and for the extensively dried trehalose sample (trehal.2) in Supplementary Material, section 1.2). These spectra show clearly that cyt *c* remains in the reduced state in all samples, providing further evidence that no redox change occurs in cyt *c* during measurements.

The XAFS oscillations measured for all samples are shown in Fig. 3 (*continuous lines*). Only small differences (mainly around 8 $Å^{-1}$) are detectable in the spectra of the solutions in the absence (sol. 1) and in the presence (sol. 2) of glycerol and the PVA sample. The most evident change is observed in the extra-dry trehalose matrix (trehal.2). This sample exhibits a large increase of the oscillation at ~11.5 $Å^{-1}$. Changes are also evident around 8 $Å^{-1}$ as well as at 5 $Å^{-1}$ where higher frequencies appear. Moreover, damping of oscillations at increasing *k* values is strongly reduced in the extensively dried trehalose sample. Far less evident changes are detectable in the moderately dried trehalose matrix. Some features of this sample seem to indicate an intermediate situation between the extensively dried trehalose matrix and solution or PVA matrix: the two oscillations at 8 $Å^{-1}$, clearly detectable in trehal.2, start to separate in trehal.1, and the signal is more structured at high *k* values as compared to the solution or PVA samples. These qualitative observations suggest that the local structure and dynamics of the iron site in ferrocyt *c* is only marginally affected by the presence of glycerol in solution or by incorporation of the protein into a solid PVA matrix. Therefore, we expect the XAFS signals of the solution and PVA samples not to differ substantially from a signal generated ab initio from the reference model structure described under Materials and Methods, obtained from XAFS data of ferrocyt in a water/glycerol mixture (38). Instead, significant differences in the structure and dynamics of the ligand cluster can be reasonably expected for the trehalose matrices. The strongly reduced damping of oscillations suggests, in fact, that incorporation into an extensively dried trehalose matrix substantially affects the DW factors. At the same time, some of the spectral changes detected in the trehalose matrices (see above) may result from significant structural modifications of the ligand cluster induced by a strong protein-matrix interaction.

In analyzing these matrix effects it is important to discriminate between changes in the XAFS signal determined

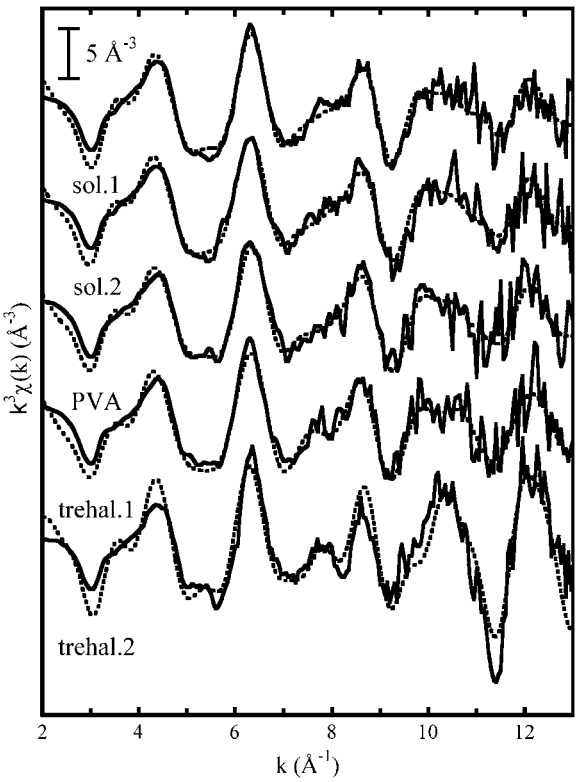

FIGURE 3 Experimental k^3-weighted XAFS signals for all measured samples (*continuous lines*). From the top to the bottom: protein in solution without (sol. 1) and with glycerol (sol. 2), protein embedded in the polyvinyl alcohol film (PVA), in the moderately dried trehalose matrix (trehal. 1), and in the extensively dried trehalose matrix (trehal. 2). The dashed lines represent calculated best fitting XAFS signals, corresponding to the parameters reported in Table 2. See text for details.

by variations in the DW factors or in the interatomic distances. We found ab initio XAFS simulations to be particularly useful to disentangle dynamic from structural contributions and proceeded as follows. Simulations were performed by fixing the atomic coordinates according to the reference structural model (see Materials and Methods). As far as values of the DW factors are concerned, five different models were considered. In the first one, all the DWs were set equal to zero, thus without any treatment of disorder; in the second one, DW values were selected on the basis of literature results (26,38,39,46–49) to mimic the dynamic behavior expected for a protein embedded in a noninteracting medium at room temperature: DW (N_p) = 2.5×10^{-3} $Å^2$; DW ($N_{\varepsilon 2}$) = 3.5×10^{-3} $Å^2$; DW (S_δ) = 5.0×10^{-3} $Å^2$; DW ($C_{2,3,4,5}$) = 3.0×10^{-3} $Å^2$; DW (C_6) = DW ($C_{\varepsilon 1}$,$C_{\delta 2}$,C_γ,$N_{\delta 1}$) = 4.0×10^{-3} $Å^2$. The value of the other single and multiple scattering DWs was 0.01 $Å^2$. In addition to these two models we built three other sets of DW factors, intermediate between models 1 and 2, in which, having fixed to zero the DW factors of the first ligands only, an increasing additional partial damping was introduced in the relative mean-square displacements of more distant shells. The

results of these five simulations are shown in Supplementary Material, section 2. Changing the DW factors, besides affecting the damping of the main oscillation, causes limited modifications mainly in the region where higher oscillations appear (8 and 10 $Å^{-1}$). A comparison with experimental signals (cf. Fig. 3 and Supplementary Material, section 2) shows that model 2 reproduces more reasonably the main features of the spectra measured in solution (sol. 1, sol. 2) and in the PVA matrix (PVA). None of the simulated signals, however, exhibits the clear separation of the two peaks at 8 $Å^{-1}$, which is observed experimentally in the extensively dried trehalose matrix (trehal.2). Moreover, in all the simulations, the amplitude of the negative peak at 9 $Å^{-1}$ is comparable to or larger than that of the peak at 11 $Å^{-1}$. Just the opposite occurs in the spectrum measured in the extra-dry trehalose sample, which exhibits a peak at 11 $Å^{-1}$ largely exceeding in amplitude that at 9 $Å^{-1}$. It appears, therefore, that a decrease of the DW factors, which of course can account for the decreased damping of oscillation observed in the trehalose matrices, is unable to reproduce some prominent features of the spectrum measured in the extensively dried sugar sample. These observations suggest that in trehalose the protein experiences, along with an enhanced local order, significant structural distortions.

Analysis of the simulated spectra in terms of the partial contributions arising from the different scattering paths can provide useful hints in identifying putative structural changes responsible for the spectral modifications observed in the trehalose samples. Fig. 4 shows the simulation performed on the basis of the reference structure using the DW factors of model 1 (*dashed line*) and model 2 (*continuous line*) described above, together with the eight main partial contributions. They all come from the heme structure. A quantitative inspection of the relative amplitudes of all the contributions confirms that the spectrum is dominated by paths involving atoms of the heme group. This appears to be a general property of heme proteins (44). It suggests that the XAFS signal is only weakly sensitive to structural modifications involving atoms not belonging to the heme structure. As to the axial ligands histidine and methionine, we noticed that the first ligand contributions involving these residues have an amplitude that is comparable to that of some MS heme paths, whereas the single scattering and MS contributions involving the most distant atoms of the histidine and methionine are all below 15% relative to the contribution of greatest amplitude.

Effects caused by changes in the orientation of the histidine residue relative to the heme group have been explored by performing a series of simulations in which bending of the imidazole group, in-plane tilting of the histidine, and twisting around the heme axis by angles of 10° and 20° were considered independently (see Supplementary Material, section 3). In the case of twisting movements, moderate alterations are induced at low k values. Interestingly, bending and twisting movements induce small spectral

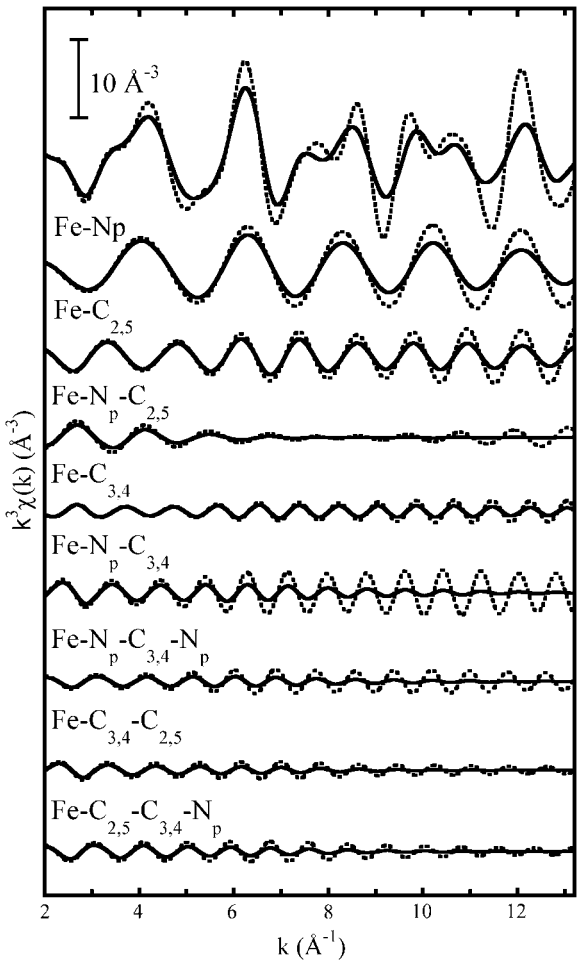

FIGURE 4 Simulations based on the reference structural model (see Fig. 1). The values of the DW factors have been fixed as in models 1 (*dashed line*) and 2 (*continuous line*) (see text for details). Together with the total XAFS signal (*top*), we show the main partial contributions.

changes, again in the region around 8 $Å^{-1}$. However, we found that all the orientation changes tested had only moderate effects on the spectrum, and in no case were they able to reproduce the characteristic features of trehalose matrices. Also, when these simulations were performed trying different sets of DW factors (not shown), the same conclusion was reached. Similar tests were performed for the methionine residue, and it was found that the effect of the angular distortions was even weaker (not shown).

When the relative contributions of the different scattering paths for the reference model structure are examined (see Fig. 4), it is clear that the main oscillation of the spectrum is caused by the four pyrrolic nitrogens of the porphyrin group. Because this oscillation does not show significant phase changes in the different samples (cf. Fig. 3), we infer that the heme first ligand distances also should not change markedly when the protein is embedded in the trehalose matrices. To explain the spectral alterations observable in the sugar samples, we are left with the possibilities that they are caused

by changes of histidine or methionine first ligand distances and/or by structural distortions of the higher shells of the heme group. Because the spectrum is essentially determined by the heme structure, the possibility that a variation of the first ligand distance of the axial residues can account by itself for the strong spectral alterations that characterize the extensively dried trehalose sample is unlikely.

In summary, the results of these ab initio simulations yield the following guidelines in selecting appropriate fitting procedures:

1. A rigid body refinement analysis, based on the reference model described under Materials and Methods, is expected to account adequately for the spectra in solution and in PVA.
2. Neither changes in disorder parameters nor the considered rotations of histidine and methionine seem sufficient to mimic the prominent features observed in the extensively dried trehalose matrix. Besides possible variations in the first ligand distance of histidine and/or methionine, strereochemical distortions of the heme group have to be considered, thus releasing the constraint of rigid body refinement.

In view of this last indication, when analyzing spectra obtained in the trehalose matrices (trehal.1 and trehal.2), we inserted three additional degrees of freedom, grouping together the porphyrin atoms ($C_{2,5}$, C_6, $C_{3,4}$) in three shells along with the first one and letting the corresponding distances from the iron vary independently. The detailed fitting procedures have been described under Materials and Methods.

In Table 2 we report the structural parameters and the corresponding *R*-factors we have determined for the five samples following the procedures described above. As shown in Fig. 3, good fits (*dashed lines*) were obtained for all samples. For the samples not embedded in trehalose matrices, the best fits were obtained using rigid body refinement keeping the values of the bending angles $FeN_{\varepsilon 2}C_{\delta 2}$ and $FeS_{\delta}C_{\varepsilon,\gamma}$ for the histidine and methionine residues, respectively (see Fig. 1 *B*), fixed to the ones of the reference model. Allowing the histidine and methionine bending angles to vary as free parameters did not improve the fit, confirming the validity of the reference model.

TABLE 2 Structural and dynamic parameters obtained for the five different matrices

	Sol. 1	Sol. 2	PVA	Trehal. 1	Trehal. 2
Structural parameters: interatomic distances (Å)					
Fe-N_p	1.99 (2)	1.99 (2)	1.99 (2)	1.99 (1)	1.991 (9)
Fe-$N_{\varepsilon 2}$	2.10 (5)	2.10 (5)	2.10 (6)	2.20 (5)	2.29 (5)
Fe-S_{δ}	2.29 (4)	2.29 (4)	2.29 (5)	2.24 (5)	2.32 (2)
Δr $C_{2,5}$	–	–	–	0.01 (1)	0.02 (2)
Δr C_6	–	–	–	0.00 (3)	0.01 (6)
Δr $C_{3,4}$	–	–	–	0.04 (7)	0.16 (4)
Disorder parameters: Debye Waller factors (10^{-3} Å^2)					
DW (N_p)	3.6 (9)	3.2 (9)	3.1 (9)	2.3 (8)	0.0 (8)
DW ($N_{\varepsilon 2}$)	10*	20 (8)	30 (40)	2 (4)	0 (5)
DW (S_{δ})	20 (20)	20 (10)	30 (30)	10 (5)	1 (2)
DW ($C_{2,5}$)	4 (2)	5 (2)	5 (2)	4 (2)	4 (2)
DW (C_6)	8 (8)	10 (20)	8 (9)	2 (3)	4 (6)
DW ($C_{3,4}$)	10 (10)	7 (7)	6 (6)	7 (8)	2 (4)
Goodness of fit					
R-factor (%)	15	18	17	17	21

The 1 σ error on the least significant figure is reported in parentheses. Δr indicates the change in distance from Fe with respect to the reference model.

*This value was kept fixed.

Inspection of the parameters listed in Table 2 shows that there are no significant structural differences between samples in solution with and without glycerol and in the PVA matrix. When the rigid body refinement constraint was released, allowing the three distances of Fe from $C_{2,5}$, C_6, and $C_{3,4}$ to vary, fitting yielded essentially the same values for the first shell distances, and no significant variation was obtained in the three distances introduced as additional free parameters. The subtle differences observable between the solution and PVA samples in the region around 8 Å^{-1} are possibly caused by small differences in the dynamic properties of the proteins (as the simulations shown in section 2 of Supplementary Material suggest) or by small structural distortions, both involving degrees of freedom not considered in the described fitting procedure. Because these differences are close to the noise level, no further attempt to reproduce them was made.

At variance with what prevailed in the solution and PVA samples, the parameters listed in Table 2 reveal considerable structural changes in the two trehalose matrices examined. Although the Fe-N_p distance does not change (as expected), a progressive elongation of the distance between Fe and the $N_{\varepsilon 2}$ atom belonging to the imidazole ring is clearly detectable going from solution to the moderately dried (Δr-$N_{\varepsilon 2}$ = 0.1 Å) and to the extensively dried trehalose matrix (Δr-$N_{\varepsilon 2}$ = 0.2 Å). Moreover, in trehalose matrices, we detected an elongation of the fourth shell ligands of the porphyrin group that reaches 0.16 Å in the extra dry sample. Because the second ($C_{2,5}$) and the third shell (C_6) distances remain essentially unchanged (see Δr values in Table 2), the fourth shell elongation is the result of an increase of heme intraligand distances (C_2-C_3, C_4-C_5, C_3-C_4) of ~10–13% (see Fig. 5). This is a considerably high value because the maximum variation of distances for XAFS restrained refinement is usually taken to be ~10% (45,50).

The significance of the elongation in the Fe-$N_{\varepsilon 2}$ distance has been tested by fitting XAFS signals of all the samples to alternative, simplified models in which the number of parameters was reduced. Specifically, we compared models characterized by 1), a single, common distance and DW for all five Fe-N atomic correlations, 2), two different bond lengths (Fe-N_p and Fe-$N_{\varepsilon 2}$) with a jointly refined DW factor, and 3), the two different bond lengths, each with its individual DW. The last situation corresponds to the refinements of Table 2. In the case of the trehalose samples, we

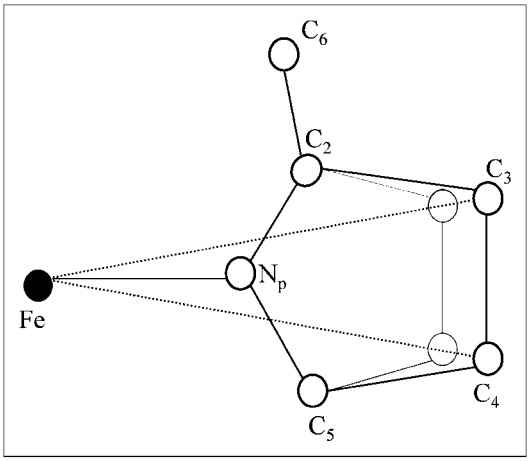

FIGURE 5 Graphic representation of the porphyrin pyrrolic group fourth shell elongation in the extra dry trehalose matrix. To obtain a simple picture we maintained the planarity of the structure, keeping collinear the Fe and $C_{3,4}$ atoms in the elongation. With these assumptions the $C_{2,5}$-$C_{3,4}$ and the C_3-C_4 distances changed by 13% and 10%, respectively.

fitted XAFS signals to models 1–3 both using rigid body refinement and releasing it, i.e., with and without the three additional degrees of freedom Δr $C_{2,5}$, Δr C_6, Δr $C_{3,4}$. The results of this analysis can be summarized as follows:

1. In sol. 1 and PVA samples, increasing the number of parameters (from model 1 to model 3) does not significantly improve the fit, so that, on a purely statistical ground, there would be no need to introduce two distinct bond lengths. However, in the case of sol. 2, i.e., in the presence of glycerol, an appreciably better fit is obtained by introducing two bond lengths with individual DWs. We note, moreover, that in solution (sol. 1 and sol. 2) and PVA, models 1 and 2 both yield problematic estimates of DW(S_δ) values (up to 10^{-1} Å^2 with uncertainties of the order of 1 Å^2). Interestingly, when a single distance is considered for all five Fe-N atomic correlations (model 1), the value of DW(N) increases by $\sim 10^{-3}$ Å^2, possibly reflecting an increase in the static disorder contribution.
2. As shown in Supplementary Material (section 4), in the case of trehalose samples (particularly in the extensively dehydrated glass, trehal.2), model 1, which assumes a unique, common (Fe-N) distance (and DW factor) for the four pyrrolic and for the histidine nitrogens, yields a definitely worse fit as compared to model 2, in which distinct (Fe-N_p) and (Fe-$N_{\varepsilon 2}$) bond lengths and a single common DW factor are considered. The fit slightly improves when individual DWs are introduced for N_p and $N_{\varepsilon 2}$. The elongation of the (Fe-$N_{\varepsilon 2}$) is already quite clear in model 2. This occurs both in rigid body refinement and with the three additional degrees of freedom, which allow for distortion in the porphyrin pyrrolic groups (see the Table in section 4 of Supplementary Material). A visual inspection of the fitting curves (see the figure in section 4 of Supplementary Material) also shows that model 1 fails to reproduce the oscillation that is observed around 8 Å^{-1}; the introduction of a distinct (Fe-$N_{\varepsilon 2}$) distance as a free parameter not only yields this oscillation but also contributes considerably to increase the amplitude of the oscillation at $\sim$11 Å^{-1}, which is a prominent feature of the trehal.2 spectrum.

The improvement of the fit described above corresponds to a decrease in both *R*-factor and reduced χ^2. From these observations we conclude that the elongation of (Fe-$N_{\varepsilon 2}$) is significant and that an (Fe-$N_{\varepsilon 2}$) bond-length distinct from the four (Fe-N_p) does not represent a redundant fitting parameter. Although in the case of sol. 1 and PVA samples, the introduction of two distinct bond lengths is not strictly required on purely statistical grounds, we also kept these degrees of freedom for the weakly interacting matrices to carry on a homogeneous comparison over the whole set of samples. We note that, in any case, this choice does not affect at all the conclusion that the (Fe-$N_{\varepsilon 2}$) bond length elongates in the trehalose glasses because in solution and PVA samples a value of 1.99(1) Å is obtained for the single (Fe-N) distance, when fitting to model 1.

As shown in Table 2, in sol. 1, sol. 2, and PVA we obtain a (Fe-$N_{\varepsilon 2}$) distance of 2.10 Å, longer than the heme (Fe-N_p) bond length (1.99 Å). Such a difference is not observable in the NMR and crystallographic structures available for cyt *c* (except for structure 1CYC, see Table 1), possibly because of their resolution limit. Comparable distances (Fe-N_p = 1.99 Å, Fe-$N_{\varepsilon 2}$ = 2.00) have been obtained in a previous XAFS study of cyt *c* (38), adopted by us as a reference model. This study was, however, performed at low temperature (10 K). The larger value for Fe-$N_{\varepsilon 2}$ resulting from our refinement is in reasonable agreement with an expected value of 2.16 Å, reported for the bond length with histidine nitrogen in an extensive compilation of metal coordination sites in proteins (http://tanna.bch.ed.ac.uk/). This value is derived from distances in the Cambridge Structural Database and partly in the PDB.

The considerable structural distortions of the Fe ligand cluster revealed by the XAFS analysis in the extensively dried trehalose matrix are in line with a number of experimental observations and with MD simulations, indicating that the trehalose matrix, upon decreasing its water content, interacts strongly with the embedded protein, significantly perturbing the energy landscape and function of the protein (16,17,22,51). On the basis of these studies, it has been proposed that the matrix-protein coupling is essentially promoted by a network of hydrogen bonds connecting groups at the protein surface, residual water molecules, and trehalose molecules (16). It is therefore conceivable that through these interactions the matrix induces conformational changes in the protein, which in turn result in structural distortions of the heme group at the

local atomic scale. Alternatively, or most likely concomitantly, the heme could be involved in a direct interaction with the matrix. Interestingly, in MD simulations performed in a nonliquid trehalose-MbCO-water system (16), one trehalose molecule has been found in persistent interaction with the heme propionate oxygen atoms. As stated in this work, this strong interaction may well induce a different configuration of the heme in the trehalose matrix with respect to the water-protein system. This interaction could be largely responsible for the elongation of the heme fourth shell detected by our analysis. In any event, our results clearly show that the protein-matrix structural interaction extends from the protein surface to a significant length scale toward the protein interior.

The effect of trehalose on the system disorder is even more dramatic (see Table 2). Although we obtained comparable values for the DW factors of first ligands for the two samples in solution and in the PVA film, the values of these parameters decrease progressively in the moderately and extensively dried trehalose matrices. In the latter, extremely low values were obtained for the pyrrolic nitrogens and for the $N_{\varepsilon 2}$ of histidine. The DW value of the methionine sulfur also undergoes a strong reduction in trehalose with respect to the value exhibited in solution and in PVA. It is worthwhile to notice that in solution and PVA the DW values of the porphyrin N_p are smaller that those of axial ligands $N_{\varepsilon 2}$ and S_δ. Although the uncertainties associated with the DW values obtained for $N_{\varepsilon 2}$ and S_δ are much larger than those for N_p, this suggests that relative motions normal to the heme plane are greater than those inside the heme plane. A similar but less pronounced difference has been reported in a previous XAFS study of ferrocyt *c* performed at 10 K (38). An analogous relation between the XAFS DW factors of the histidine $N_{\varepsilon 2}$ and of the heme pyrrolic N atoms has been obtained for met-myoglobin (26).

Because the DW factors measure the relative mean-square displacement between the absorbing and backscattering atoms only, a substantial contribution to the dramatic reduction of the Debye-Waller factors could arise from a higher correlation in the motions of the cluster atoms when the protein is embedded in dry trehalose matrices. This increased motional coherence agrees with the results of MD simulations performed on MbCO in 89% (w/w) trehalose-water (15). In fact, it was found that the deviations of the mean-square fluctuations from the linear temperature dependence above ~270 K have a similar amplitude for all the heme heavy atoms, thus suggesting that in plasticized trehalose systems the heme group, including the iron, already performs quasidiffusive motion as a whole.

XAFS studies of DW factors as a function of temperature performed on met-myoglobin (26) show that the decrease of the DW factors going from 260 K to 40 K is far less dramatic than that we observed on incorporation of the protein into a dry trehalose matrix at room temperature. Even at 40 K pyrrolic nitrogens have a DW factor of 1.9×10^{-3} Å^2 (26). The authors suggest that static disorder, resulting from a conformational structural heterogeneity of the protein, strongly contributes to the values of the DW factors at low temperature. This hypothesis is corroborated by a comparison with relative mean-square displacements calculated from normal modes, which turned out to be much smaller than the experimental ones. On this basis, we should infer that the static contribution to the disorder is also significantly decreased by the trehalose matrix. This indicates that the trehalose matrix drastically alters the protein energy landscape, hindering the protein internal dynamics and also promoting only some conformational substates at the level of local structure.

We discussed here only the DW values obtained for the first ligands. The values found for the more distant shells, although quite reasonable, are less reliable because of the approximations of the model. We recall, in fact, that for higher-order shells, only the DW factor of the porphyrin group was allowed to vary (see Materials and Methods). Therefore, caution is needed, in particular in the case of samples inserted in trehalose. The values of the fixed DW factors (0.01 Å^2, see Materials and Methods) might no longer be reliable in the trehalose matrices. If this is the case, because MS contributions are very important at distances >3 Å, differences in their DW factors can lead to a poor estimate of the free DW values. Hence, it is rather risky to make conclusions based on these values. However, it should be noticed that in the extra dry trehalose matrix the relative mean-square displacements of the porphyrinic outer shells are also lower when compared to those found in solution. Interestingly, in this matrix the fourth shell value ($DW(C_{3,4})$) seems to be lower than that related to the second shell ($DW(C_{2,5})$), at variance with all the other matrices, where the opposite is true. The larger decrease in $DW(C_{3,4})$ might reflect the strong interaction with the matrix that is responsible for the structural change localized at the same $C_{3,4}$ atoms.

CONCLUSIONS

The reported XAFS analysis of cyt *c* in different solvent/matrix systems indicates that incorporation of the protein into an extensively dehydrated trehalose matrix has strong effects on the structure and dynamics of the Fe ligand cluster. Although essentially the same structural and disorder parameters account for the XAFS spectra measured in aqueous solution, in a glycerol-water system, and when cyt *c* is embedded into a dried PVA film, incorporation into the sugar matrix results from the structural point of view in 1), an increase of the distance between Fe and the $N_{\varepsilon 2}$ atom of the histidine imidazole ring; and 2), a distortion of the heme pyrrolic units revealed by a significant elongation of the fourth-shell distance (Fe-$C_{3,4}$). Comparison between a moderately and an extremely dehydrated trehalose matrix shows that these structural distortions increase strongly when the

amount of residual water in the matrix is reduced. In fact, the elongation of the (Fe-$N_{\varepsilon 2}$) and of the (Fe-$C_{3,4}$) distances increases from 0.1 and 0.04 Å to 0.2 and 0.16 Å, respectively, when going from the less dried to the extremely dried trehalose matrix. This result is in line with a number of experimental observations, performed on heme proteins and on photosynthetic reaction centers, which clearly indicate a critical dependence of structural/dynamic and functional effects on the hydration state of the embedding trehalose matrix (19).

It is noteworthy that, at variance with the large effects observed in the sugar matrices, incorporation of the protein in a dehydrated PVA film does not lead to any relevant change in the structural and disorder parameters of the Fe ligand cluster as compared to solution. This finding, indicating a very weak structure/dynamics coupling between the protein and the PVA matrix, is consistent with the observation that incorporation of bacterial photosynthetic reaction centers into fully dehydrated PVA films very weakly affects the kinetics of electron transfer processes as compared to trehalose matrices (21).

The occurrence of structural distortions of the heme group when a heme protein interacts with a trehalose matrix has been suggested by spectral diffusion studies in cyt *c* (18) and inferred on the basis of MD simulations of a water-trehalose-MbCO amorphous system (15,16). In the case of cyt *c,* our analysis lets us identify and resolve these proposed structural effects at the atomic scale. The obtained elongation of the distance between Fe and the coordinating histidine N atom, as well as the strong distortion of the heme pyrrolic geometry, testify to a very tight structure/dynamics coupling between the matrix and the protein in trehalose systems. Indeed, disorder parameters obtained from XAFS analysis evidence a parallel severe decrease in the relative mean-square displacements of the Fe first ligand atoms, which becomes dramatic in the extensively dried trehalose matrix. This finding is in full agreement with the results of experimental studies and MD simulations performed on trehalose-coated MbCO, all indicating a drastic hindering of thermal fluctuations. Our data highlight this effect on the local Fe structure. The values of the DW factor obtained by us in solution or in the PVA compare favorably with those reported in a previous XAFS study performed on small crystals of met-myoglobin (26). However, the decrease of the DW observed in met-myoglobin on lowering the temperature to 40 K is relatively limited (26) and smaller than what we observe on incorporation of the protein into the dried trehalose matrix at room temperature. Following Scherk et al. (26), we propose that, in the case of cyt *c* also, static structural heterogeneities resulting from a large number of coexisting protein conformations give a substantial contribution to the values of the DW factors obtained in solution or in the PVA film. The dramatic reduction of the relative mean-square displacement found in the extensively dried trehalose would therefore reflect not only a reduction of dynamics, possibly resulting from an increased coherence in the motions of the cluster atoms, but, to a considerable extent, a decreased static disorder as well. If this is the case, it appears that incorporation into an extremely dried trehalose matrix, by drastically affecting the energy landscape of cyt *c*, selects a restricted number of conformational substates at the level of local structure.

SUPPLEMENTARY MATERIAL

An online supplement to this article can be found by visiting BJ Online at http://www.biophysj.org.

We are grateful to the staff of the GILDA beamline of ESRF for excellent support. L.G. acknowledges EMBO for supporting her participation in the school ''BioXAS Practical Course on metalloproteins and organism tissue'' (EMBL, Hamburg, June 14—19, 2005).

This work was supported by MIUR of Italy (grant PRIN 2005, Proprietà Dinamiche Strutturali e Funzionali di Proteine in Sistemi Non-Liquidi Contenenti Acqua Residua: Accoppiamento con la Matrice Esterna). Measurements at ESRF were performed within the public user program.

REFERENCES

1. Leslie, S. B., E. Israeli, B. Lighthaert, J. H. Crowe, and L. M. Crowe. 1995. Trehalose and sucrose protect both membranes and proteins in intact bacteria during drying. *Appl. Environ. Microbiol.* 91:3592–3597.
2. Uritani, M., M. Takai, and K. Yoshinaga. 1995. Protective effect of disaccharides on restriction endonucleases during drying under vacuum. *J. Biochem. (Tokyo).* 117:774–779.
3. Sun, W. Q., and P. Davidson. 1998. Protein inactivation in amorphous sucrose and trehalose matrices: effects of phase separation and crystallization. *Biochim. Biophys. Acta.* 1425:235–244.
4. Crowe, J. H., J. F. Carpenter, and L. M. Crowe. 1998. The role of vitrification in anhydrobiosis. *Annu. Rev. Physiol.* 60:73–103.
5. Crowe, L. M. 2002. Lessons from nature: the role of sugars in anhydrobiosis. *Comp. Biochem. Physiol. A.* 131:503–513.
6. Carpenter, J. F., and J. H. Crowe. 1989. An infrared spectroscopic study of the interaction of carbohydrates with dried proteins. *Biochemistry.* 28:3916–3922.
7. Belton, P. S., and A. M. Gil. 1994. IR and Raman spectroscopic studies of the interaction of trehalose with hen egg white lisozyme. *Biopolymers.* 34:957–961.
8. Sampedro, J. G., and S. Uribe. 2004. Trehalose-enzyme interactions results in structure stabilization and activity inhibition. *Mol. Cell. Biochem.* 256:319–327.
9. Green, J. L., and C. A. Angell. 1989. Phase relations and vitrification in saccharide-water solutions and trehalose anomaly. *J. Phys. Chem.* 93:2880–2882.
10. Cordone, L., P. Galajada, E. Vitrano, A. Gassmann, A. Ostermann, and F. Parak. 1998. A reduction of protein specific motions in co-ligated myoglobin embedded in a trehalose glass. *Eur. Biophys. J.* 27:173–176.
11. Parak, F., E. W. Knapp, and D. Kucheida. 1982. Protein dynamics. Mössbauer spectroscopy on deoxymyoglobin crystals. *J. Mol. Biol.* 161:177–194.
12. Cordone, L., M. Ferrand, E. Vitrano, and G. Zaccai. 1999. Harmonic behavior of trehalose-coated carbon-monoxy-myoglobin at high temperature. *Biophys. J.* 76:1043–1047.
13. Doster, W., S. Cusack, and W. Petry. 1989. Dynamical transition of myoglobin revealed by inelastic neutron scattering. *Nature.* 337:754–756.

14. Köper, I., M. C. Bellissent-Funel, and W. Petry. 2000. Influence of trehalose on the dynamics of a protein: the C-phycocyanin. *Eur. Biophys. J.* 29:263 (Abstr.)

15. Cottone, G., L. Cordone, and G. Ciccotti. 2001. Molecular dynamics simulation of carboxy-myoglobin embedded in a trehalose-water matrix. *Biophys. J.* 80:931–938.

16. Cottone, G., G. Ciccotti, and L. Cordone. 2002. Protein-trehalose-water structures in trehalose coated carboxy-myoglobin. *J. Chem. Phys.* 117:9862–9866.

17. Giuffrida, S., G. Cottone, F. Librizzi, and L. Cordone. 2003. Coupling between the thermal evolution of heme pocket and external matrix structure in trehalose coated carboxy-myoglobin. *J. Phys. Chem. B.* 107:13211–13217.

18. Ponkratov, V. V., J. Friedrich, and J. M. Vanderkooi. 2002. Solvent effects on conformational dynamics of proteins: cytochrome *c* in a dried trehalose film. *J. Chem. Phys.* 117:4594–4601.

19. Cordone, L., G. Cottone, S. Giuffrida, G. Palazzo, G. Venturoli, and C. Viappiani. 2005. Internal dynamics and protein-matrix coupling in trehalose-coated proteins. *Biochim. Biophys. Acta.* 1749:252–281.

20. Palazzo, G., A. Mallardi, A. Hochkoeppler, L. Cordone, and G. Venturoli. 2002. Electron transfer kinetics in photosynthetic reaction centers embedded in trehalose glasses: trapping of conformational substates at room temperature. *Biophys. J.* 82:558–568.

21. Francia, F., L. Giachini, G. Palazzo, A. Mallardi, F. Boscherini, and G. Venturoli. 2004. Electron transfer kinetics in photosynthetic reaction centers embedded in polyvinyl alcohol films. *Bioelectrochemistry.* 63:73–77.

22. Francia, F., G. Palazzo, A. Mallardi, L. Cordone, and G. Venturoli. 2003. Residual water modulates Q_A^- to Q_B electron transfer in bacterial reaction centers embedded in trehalose amorphous matrices. *Biophys. J.* 85:2760–2775.

23. Koninsgsberger, D. C., and R. Prins. 1988. X-ray absorption: principles, applications, techniques of EXAFS, SEXAFS and XANES. Wiley, New York.

24. Samar Hasnain, S., and K. O. Hodgson. 1999. Structure of metal centres in proteins at subatomic resolution. *J. Synchr. Rad.* 6:852–864.

25. Beni, G., and P. M. Platzman. 1976. Temperature and polarization dependence of extended x-ray absorption fine-structure spectra. *Phys. Rev. B.* 14:1514–1518.

26. Scherk, C. G., A. Ostermann, K. Achterhold, O. Iakovleva, C. Nazikoll, B. Krebs, E. V. Knapp, W. Meyer-Klaucke, and F. G. Parak. 2001. The x-ray absorption spectroscopy Debye-Waller factors of an iron compound and met-myoglobin as a function of temperature. *Eur. Biophys. J.* 30:393–403.

27. Pascarelli, S., F. Boscherini, F. D'Acapito, J. Hardy, C. Meneghini, and S. Mobilio. 1996. X-ray optics of a dynamical sagittal focussing monochromator on the GILDA beamline at the ESRF. *J. Synchr. Rad.* 3:147–155.

28. Ciatto, G., F. D'Acapito, F. Boscherini, and S. Mobilio. 2004. Treatment of EXAFS data taken in the fluorescence mode in non-linear conditions. *J. Synchr. Rad.* 11:278–283.

29. Tanaka, N., T. Yamane, T. Tsukihara, T. Ashida, and M. Kakudo. 1975. The crystal structure of bonito (katsuo) ferrocytochrome *c* at 2.3 Å resolution. II. Structure and function. *J. Biochem. (Tokyo).* 77:147–162.

30. Takano, T., and R. E. Dickerson. 1980. Redox conformation changes in refined tuna cytochrome *c*. *Proc. Natl. Acad. Sci. USA.* 77:6371–6375.

31. Ochi, H., Y. Hata, N. Tanaka, M. Kakudo, T. Sakurai, S. Aihara, and Y. Morita. 1983. Structure of rice ferricytochrome *c* at 2.0 Å resolution.. *J. Mol. Biol.* 166:407–418.

32. Takano, T. 1984. Refinement of myoglobin and cytochrome *c*. *In:* Methods and Applications in Crystallographic Computing. S. R. Hall, and T. Hashida, editors. Oxford University Press, Oxford. 262–272.

33. Bushnell, G. W., G. V. Louie, and G. D. Brayer. 1990. High-resolution three-dimensional structure of horse heart cytochrome *c*. *J. Mol. Biol.* 214:585–595.

34. Sanishvili, R., K. W. Volz, E. M. Westbrook, and E. Margoliash. 1995. The low ionic strength crystal structure of horse cytochrome *c* at 2.1 Å resolution and comparison with its high ionic strength counterpart. *Structure.* 3:707–716.

35. Qi, P. X., R. A. Beckman, and A. J. Wand. 1996. Solution structure of horse heart ferricytochrome *c* and detection of redox-related structural changes by high-resolution ^{1}H NMR. . *Biochemistry.* 35:12275–12286.

36. Banci, L., I. Bertini, J. G. Huber, G. A. Spyroulias, and P. Turano. 1999. Solution structure of reduced horse heart cytochrome *c*. *J. Biol. Inorg. Chem.* 4:21–31.

37. Bartalesi, I., I. Bertini, P. Hajieva, A. Rosato, and P. R. Vasos. 2002. Solution structure of a monoheme ferrocytochrome *c* from *Shewanella putrefaciens* and structural analysis of sequence-similar proteins: functional implications. . *Biochemistry.* 41:5112–5119.

38. Cheng, M., A. M. Rich, R. S. Armstrong, P. J. Ellis, and P. A. Lay. 1999. Determination of iron-ligand bond lengths in ferric and ferrous horse heart cytochrome *c* using multiple-scattering analyses of XAFS data. *Inorg. Chem.* 38:5703–5708.

39. Rich, A. M., R. S. Armstrong, P. J. Ellis, H. C. Freeman, and A. Lay. 1998. Determination of iron-ligand bond lengths in horse heart met- and deoxymyoglobin using multiple-scattering XAFS analyses. *Inorg. Chem.* 37:5743–5753.

40. Newville, M., P. Livins, Y. Yacoby, E. A. Stern, and J. J. Rehr. 1993. Near-edge x-ray-absorption fine structure of Pb: a comparison of theory and experiment. *Phys. Rev. B.* 47:14126–14131.

41. Ravel, B., and M. Newville. 2005. ATHENA, ARTEMIS, HEPHAESTUS: data analysis for x-ray absorption spectroscopy using IFEFFIT. *J. Synchr. Rad.* 12:537–541.

42. Ankudinov, A. L., B. Ravel, J. J. Rehr, and S. D. Conradspon. 1998. Real space multiple-scattering calculation and interpretation of x-ray-absorption near-edge structure. *Phys. Rev. B.* 58:7565–7576.

43. Pin, S., B. Alpert, A. Congiu-Castellano, S. D. Longa, and A. Bianconi. 1994. X-ray absorption spectroscopy of hemoglobin. *Meth. Enzym.* 232:266–292.

44. Levina, A., R. S. Armstrong, and P. A. Lay. 2005. Three-dimensional structure determination using multiple-scattering analysis of XAFS: applications to metalloproteins and coordination chemistry. *Coord. Chem. Rev.* 249:141–160.

45. Binsted, N., R. W. Strange, and S. S. Hasnain. 1992. Constrained and restrained refinement in EXAFS data analysis with curved wave theory. *Biochemistry.* 31:12117–12125.

46. Cheung, K., R. Strange, and S. S. Hasnain. 1999. 3D EXAFS refinement of the Cu site of azurin sheds light on the nature of structural change at the metal centre in an oxidation-reduction process: an integrated approach combining EXAFS and crystallography. *Acta Crystallogr. D.* 56:697–704.

47. Dimakis, N., and G. Bunker. 2001. Chemical transferability of single and multiple-scattering EXAFS Debye-Waller factors. *J. Synchr. Rad.* 8:297–299.

48. Dimakis, N., and G. Bunker. 2002. Group-fitted ab initio single- and multiple-scattering EXAFS Debye-Waller factors. *Phys. Rev. B.* 65: 201103.

49. Dimakis, N., and G. Bunker. 2004. XAFS Debye-Waller factors for Zn metalloproteins. *Phys. Rev. B.* 70:195114.

50. Engh, R., and R. Huber. 1991. Accurate bond and angle parameters for x-ray protein structure refinement. *Acta Crystallogr. A.* 47:392–400.

51. Librizzi, F., C. Viappiani, S. Abbruzzetti, and L. Cordone. 2002. Residual water modulates the dynamics of the protein and of the external matrix in ''trehalose coated'' MbCO: an infrared and flash-photolysis study. *J. Chem. Phys.* 116:1193–1200.